chemistry

MDPI

Review

Complementarity and Preorganisation in the Assembly of Heterometallic–Organic Cages via the Metalloligand Approach—Recent Advances

Feng Li [1,*] and Leonard F. Lindoy [2,*]

[1] School of Science, Western Sydney University, Penrith, NSW 2751, Australia
[2] School of Chemistry, The University of Sydney, Camperdown, NSW 2006, Australia
* Correspondence: feng.li@westernsydney.edu.au (F.L.); leonard.lindoy@sydney.edu.au (L.F.L.)

Abstract: The design of new metallocage polyhedra towards pre-determined structures can offer both practical as well as intellectual challenges. In this mini-review we discuss a selection of recent examples in which the use of the metalloligand approach has been employed to overcome such challenges. An attractive feature of this approach is its stepwise nature that lends itself to the design and rational synthesis of heterometallic metal–organic cages, with the latter often associated with enhanced functionality.

Keywords: metalloligand; metal–organic cage; metallocage; heterometal; template

Citation: Li, F.; Lindoy, L.F. Complementarity and Preorganisation in the Assembly of Heterometallic–Organic Cages via the Metalloligand Approach—Recent Advances. *Chemistry* **2022**, *4*, 1439–1456. https://doi.org/10.3390/chemistry4040095

Academic Editor: Craig Rice

Received: 29 September 2022
Accepted: 5 November 2022
Published: 7 November 2022

1. Introduction

Starting with an initial report of the synthesis of a metal–organic cage (MOC) more than three decades ago [1], creativity, often coupled with serendipity, has played a major role in the construction of a vast array of MOCs displaying diverse topologies that are often associated with interesting properties. The resulting MOCs consist of hollow polyhedral 3D structures in which the metal ion nodes are commonly linked by bi- or multi-functional organic linkers that also serve to define the sides of the polyhedron.

Such cages include both homo- and heterometallic derivatives, with the majority incorporating d- and/or f-block transition or (less commonly) main group metal ions as structural elements [2–8]. The nature of the metal ions, including their size, charge, electronic configuration, stereochemical preferences, kinetic labilities, and donor–atom binding preferences are all parameters available for use in "tuning" individual cage structures and, hence, also their properties. MOCs have been demonstrated to show varying degrees of porosity as well as some degree of flexibility. Such porosity/flexibility has long been known to be an important factor influencing the ease of ingress and egress of guests into and out of the cavity [9]. Indeed, the host–guest chemistry of MOCs continues to receive extremely wide attention [10–22], with individual cages frequently displaying a range of properties that include both photoactive [23–26] and magnetic [27–33] behaviours.

Many promising applications for individual cages have now been investigated [34–37]. These include applications for sequestering a wide range of both ions and molecules [38–41]; for molecule and ion sensing [23,42–55]; for the stabilisation of reactive species [56,57]; for catalysis where the cage acts as a "reaction vessel" in which, for example, the proximity of the reactants (amongst other influences) act as a driver for promoting enhanced reaction rates [58–75]; as well as for use in biochemical applications [76,77] that include MRI imaging [78], photodynamic therapy [79], and ion/molecule (including drug) transport [80–84].

Over recent years the complexity, diversity, and functionality of reported MOCs have all tended to increase, in part resulting from the availability of an expanded array of innovative synthetic protocols [85–96] that include the metalloligand approach [97–100].

In this mini-review, recent examples of the design, synthesis, and properties of selected discrete heterometal–organic cages whose assembly involves the use of a metalloligand strategy are discussed. Metalloligands have now been widely employed for the rational assembly of an extensive range of MOCs; in particular, this "complex as a ligand" approach lends itself to the construction of heterometallic cages, consequently engendering both additional complexity and potential functionality to such systems. The following discussion is designed to be illustrative rather than comprehensive, with emphasis given to systems chosen from the more recent literature.

2. Metalloligand Strategies for the Assembly of MOCs

Metalloligands typically employed in polynuclear cage assembly formation can be grouped into two main categories [97]. The first group corresponds to systems in which the metalloligand's bound (primary) metal ion acts to orientate initially non-bonded donor atoms so that they are suitably aligned for binding to further (secondary) metal ions and lead to cage formation. This process may also involve the use of co-ligands, if needed, to satisfy the coordination requirements of the secondary metal ions involved in cage formation. The second category consists of metalloligands that incorporate a bound primary metal ion (or ions) with the latter not primarily involved in orienting further unbound metal–ion donor sites for cage formation. Systems of this latter type are not included in the following discussion.

2.1. Metalloligand Systems Incorporating a Bound Primary Metal Ion That Sterically Organises Initially Unbound Secondary Donor Atoms for Cage Formation

In situ 2:1 Schiff base condensation reaction between 1-(pyridine-4-yl)-1H-imidazole-4-carbaldehyde and 1,4-diaminopropane in the presence of copper(II) nitrate in acetonitrile results in formation of the V-shaped Cu(II) complex **1**. Inherent in the design of this species is the presence of two fully conjugated moieties linked by a flexible trimethylene bridge such that, on binding to Cu(II), the two terminal 4-pyridyl groups are oriented in a divergent manner such that, on acting as a metalloligand, they are unable to bind simultaneously to a single metal ion. The use of **1** as a metalloligand has been shown to generate a $[Pd_4Cu_8]^{24+}$ partially face-centred cubic structure of type $[Pd_4(CuL)_8(H_2O)_6(DMSO)_2](NO_3)_{24}$ (**2**) [where CuL^{2+} = metalloligand **1** and DMSO = dimethyl sulfoxide)] [101]. This was achieved by a 2:1 reaction of **1** with Pd(II), with the latter having a well-documented propensity for pyridyl nitrogen coordination as well as for the adoption of a square planar coordination geometry. The crystal structure of this cationic cage resembles a cubic box with two opposing faces not capped by Pd(II) ions (see Figure 1).

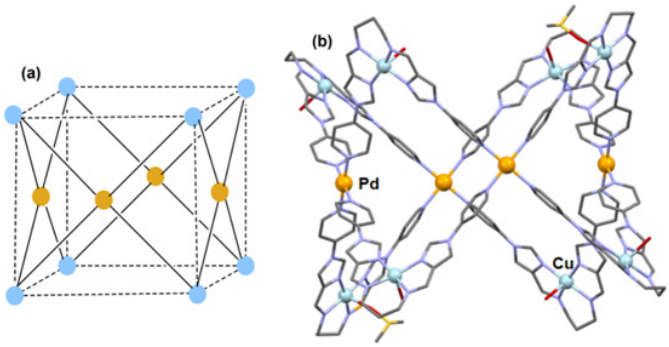

Figure 1. Structural details of the cubic cation in $[Pd_4(CuL)_8(DMSO)_2(H_2O)_6](NO_3)_{24}$ (**2**), where $[CuL]^{2+}$ is the metalloligand **1**. (**a**) Schematic representation of the metal ion sites in the partially face-centred cube. (**b**) Crystal structure of the cubic cation showing the square pyramidal coordination of each copper(II) centre and the square planar geometry of each palladium(II) centre which is bound to four pendent 4-pyridyl groups. Hydrogen atoms, lattice solvent molecules, and nitrate counterions are not shown [101].

Clearly, this outcome reflects the presence of only two secondary donor sites available in each metalloligand of type **1** rather than the three present in the tripodal metalloligands discussed later in this section (and which form fully face-centred $M_6M'_8$ cube structures).

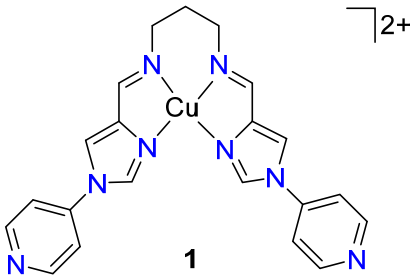

1

Each copper(II) centre adopts a 5-coordinate square-pyramidal geometry with the basal plane defined by four pyridyl nitrogen donors while each axial position is occupied by an oxygen donor from a water or dimethyl sulfoxide ligand. This square box molecule was demonstrated to act as an efficient catalyst for the epoxidation of styrene and its derivatives, with the presence of opposing open sides in this structure proposed to aid catalytic activity by allowing facile substrate diffusion in and out of the cavity.

Reaction of the difunctional metalloligand $[Ru(dtbubpy)_2(qpy)]^{2+}$ (**3**) (2 equiv., as its PF_6^- salt) with palladium(II) (1 equiv.) in dimethyl sulfoxide (DMSO) $[Ru_8Pd_4]^{24+}$ yielded a cubic cage of type $[Ru_8Pd_4(dtbubpy)_{16}(qpy)_8]^{24+}$ (**4**) (where qpy = 4,4′:2′,2″:4″,4‴-quarterpyridine and ditbubipy = 4,4′-di-tert-butyl-2,2′-bipyridine) [102]. In contrast to the copper(II) metalloligand (**1**) discussed above for **3,** the two divergent 4-pyridyl nitrogen donors are appended to an octahedral ruthenium(II) complex. Since the ruthenium centre will be kinetically inert this makes **3** a more robust metalloligand than **1**.

As anticipated, a single crystal X-ray diffraction study confirmed that the eight ruthenium(II) ions in **4** occupy the corners of the cube while the four palladium(II) ions are located on four sides, with each of these metal centres coordinated to four pyridyl groups in a square planar manner. Two (opposite) sides of the cube remain "open". The angle between the coordinated 4-pyridyl groups in the cage structure is 69°. The cage was shown to be luminescent, with a relatively high quantum yield of 6.9% for a Ru^{2+} species, given that the emission maximum occurs in the NIR at 719 nm.

In a parallel study using an analogous procedure to that above, but with 2,2–bipyridine (bipy) substituted for 4,4′-di-*tert*-butyl- 2,2′-bipyridine (dtbubpy), yielded the ruthenium(II) metalloligand **3** (with R = H; see Figure 2) which was obtained as its tetrafluoroborate salt and subsequently employed in the formation of the corresponding $[Ru_8Pd_4(bipy)_{16}(qpy)_8]^{24+}$ (where qpy = 4,4′:2′,2″:4″,4‴-quarterpyridine) cubic structure [103]. An X-ray diffraction study once again confirmed that eight ruthenium(II) ions occupy the corners of the cube while the four palladium(II) ions are positioned at the centres of four sides such that two opposing sides are again left "open". An additional feature of this study was the use of the separated optical isomers of metalloligand **3** (with R = H) in parallel reactions leading to chiral cage formation. Resolution proved feasible due to the (inherent) chemical inertness of polypyridyl ruthenium(II) species such as **3** [104]. In parallel reactions, the use of the respective resolved products on interaction with $[Pd(CH_3CN)_4]^{2+}$ resulted in two stereoisomeric cages of type Δ- or Λ-$[Ru_8Pd_4(bipy)_{16}(qpy)_8]^{24+}$ in which all eight ruthenium(II) centres in each product are associated with the same helicity; that is, they are either all right-handed (Δ Δ Δ Δ Δ Δ) or all left-handed (Λ Λ Λ Λ Λ Λ).

The metalloligand approach for cube formation is well exemplified by a series of studies by Brechen, Piligkos, and Lusby et al. in which the syntheses and investigation of heteronuclear metalloligand-based cubes of type $[M^{III}{}_8M^{II}{}_6]$ (M^{III} = Cr, Fe, Al; M^{II} = Mn, Co, Cu, Zn, Pd] were reported [105–108]. However, the studies by this group differ from those discussed so far in that the metalloligands employed were all neutral species resulting from the use of three bidentate β-diketonato ligands bound to a trivalent metal ion.

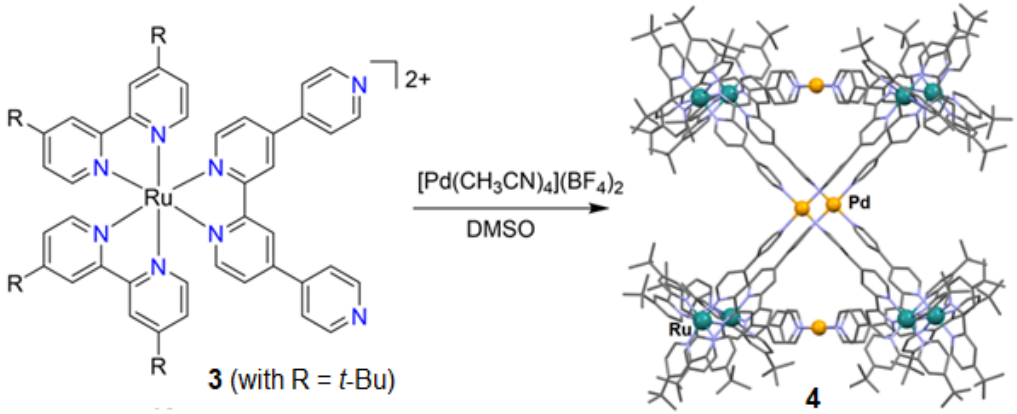

Figure 2. Synthesis and crystal structure (hydrogen atoms and BF_4^- anions are not shown) of the "open" cubic cage **4** starting from the bipodal metalloligand **3** (with R = *t*-Bu) [102].

A 2021 study by the group is representative [105]. In this, the paramagnetic, octahedral *fac*-[$Cr^{III}L_3$] complex [where LH = 1-(4-pyridyl)butane-1,3-dione)] was employed as the metalloligand for the generation of three new face-centred cubic cages. Crucial to the success of this approach was the availability of the *fac*-octahedral isomer, with its three 4-pyridyl groups arranged in a tripodal fashion directed "outwards" with respect to the central tris-β-diketonato chromium(III) core [107]. The crystal structure of this neutral, kinetically inert *fac*-[$Cr^{III}L_3$] metalloligand is shown in Figure 3.

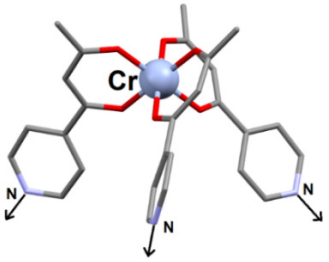

Figure 3. Crystal structure of the neutral metalloligand *fac*-[$Cr^{III}L_3$] [where LH = 1-(4-pyridyl)butane-1,3-dione)] showing the tripodal arrangement of its 4-pyridyl groups. Arrows indicate the coordination vectors of the pyridyl nitrogens [107].

Reaction of the neutral metalloligand, *fac*-[$Cr^{III}L_3$], with the appropriate nickel(II) salts resulted in the formation of the discrete heteronuclear cubic cages $[Cr^{III}_8Ni^{II}_6L_{24}(H_2O)_{12}](NO_3)_{12}$, $[Cr^{III}_8Ni^{II}_6L_{24}(CH_3CN)_7(H_2O)_5](ClO_4)_{12}$, and $[Cr^{III}_8Ni^{II}_6L_{24}Cl_{12}]$. The crystal structures of all three products were determined. In each case the eight chromium(III) ions occupy the corners of the cube while the six nickel(II) ions are positioned on the centres of its six sides. The crystal structure of $[Cr^{III}_8Ni^{II}_6L_{24}Cl_{12}]$ (which is representative of all three structures) is shown in Figure 4. Based on EPR evidence, a weak ferromagnetic interaction is present between the nickel(II) (d^8) and chromium(III) (d^3) centres in these assemblies. Similar heterometal magnetic exchange interactions between d-block metal ions in other large cage molecules are quite rare [105].

Related metalloligand strategies have also been employed to generate smaller cage systems than those discussed so far. Lützen et al. demonstrated that the low-spin, iron(II)-containing, tripodal C_3-symmetric metalloligand **5** (as its BF_4^- salt) reacts with *cis*-protected, square planar Pd(dppp)$(OTf)_2$ [where dppp = bis(diphenyl)phosphino)propane] in a 2:3 ratio in acetonitrile to form the pentanuclear trigonal bipyramidal cage **6** of composition $[(Fe^{II}L)_2\{Pd^{II}(dppp)\}_3](BF_4)_4(OTF)_6$ (where $[Fe^{II}L]^{2+}$ = **5**) (Figure 5) [109]. In assembling this smaller MOC, the two available (labile) palladium sites in each of three Pd(dppp)$(OTf)_2$ units interact with two 4-pyridyl groups from two different tripodal **5** metalloligands (Figure 5). On forming **6**, the octahedral geometry of the iron(II) sites as well

as the square planar geometry of the palladium(II) sites present in the precursor complexes are both preserved. Clearly, central to successful trigonal bipyramidal cage formation, in this case, is the use of the *cis*-protected square planar precursor Pd(dppp)$(OTf)_2$.

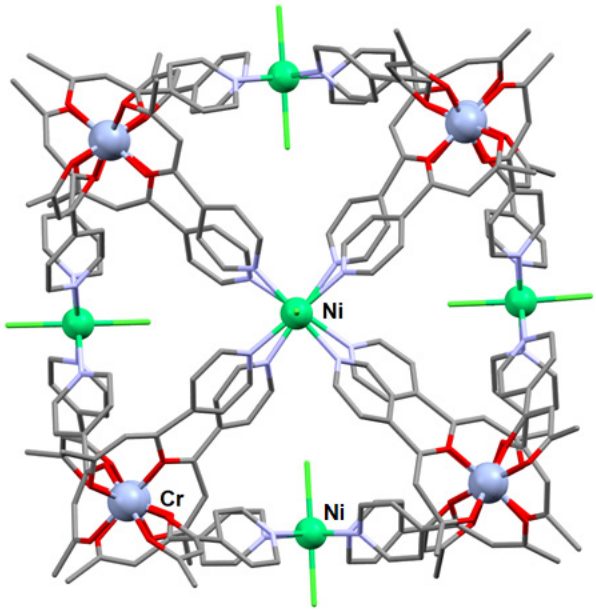

Figure 4. Crystal structure of $[Cr^{III}{}_8Ni^{II}{}_6L_{24}Cl_{12}]$, where LH = 1-(4-pyridyl)butane-1,3-dione. The green sticks represent chlorido ligands and the red sticks oxygen donor atoms. Hydrogen atoms are not shown [105].

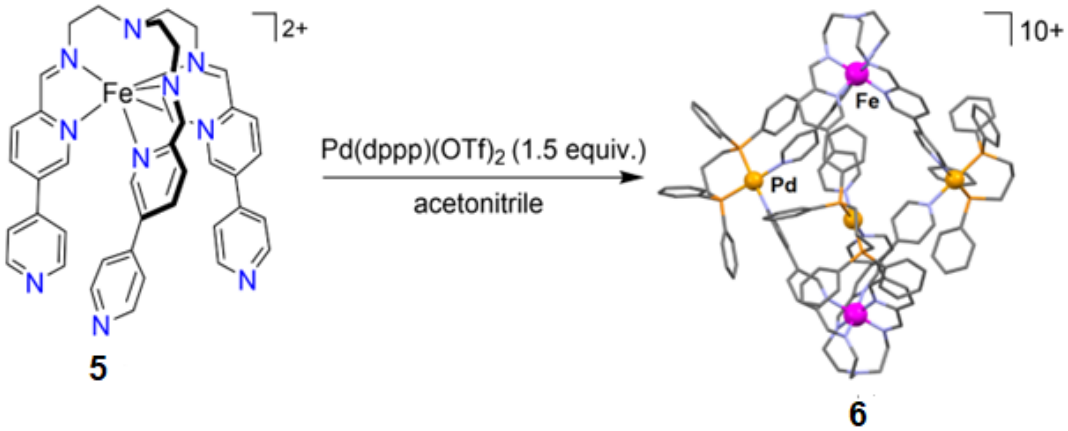

Figure 5. Assembly of the $[(Fe^{II}L)_2\{Pd^{II}(dppp)\}_3]^{10+}$ cation **6** from metalloligand **5** and $Pd^{II}(dppp)(OTf)_2$ [109].

When non-*cis*-protected $[Pd(CH_3CN)_4](BF_4)_2$ was employed for reaction with **5**, then the larger tetradecanuclear $[Fe_8{}^{II}Pd_6{}^{II}L_8]^{28+}$ (where $[FeL]^{2+}$ = **5**) face-centred cubic cage was generated. While no X-ray structure determination was obtained for this product, its cubic structure was assigned from NMR (^1H, ^{13}C, DOSY), UV-Vis spectroscopy and ESI–MS measurements; iron(II) centres occupy the corners of the cube while palladium(II) centres are located on each of its six faces. Once again, in this structure both the iron(II) and palladium(II) centres display their most common coordination geometries in accord with this being a driver influencing the formation of both cage topologies generated in this study.

In a further study, the Lützen group employed the sterically modified iron(II) metalloligand **7**, incorporating a methyl substituent on each of its tripodal arms [110]. This more

bulky metalloligand species was obtained by reaction of 2-formyl-6-methylpyridine with tris(2-aminoethyl)amine and iron(II) tetrafluoroborate in acetonitrile; the tripodal structure of the product was confirmed by X-ray diffraction. The presence of steric hindrance arising from the methyl substituents was sufficient to result in a lowering of the effective ligand field towards the bound iron(II) centre, and the latter is high-spin at room temperature, contrasting with the low-spin state that occurs in the unsubstituted iron(II) analogue **5**.

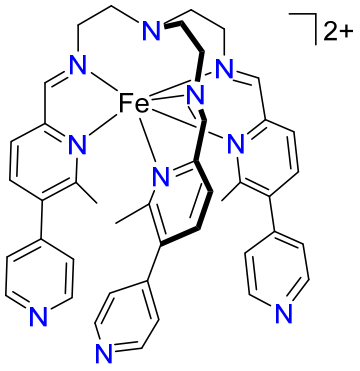

7

Reaction of the metalloligand **7** (1 equiv.) with Pd(dppp)$(OTf)_2$ (1.5 equiv.) in acetonitrile resulted in formation of the pentanuclear trigonal bipyramidal cage in which palladium(II) centres lie in the triangular equatorial plane of the bipyramid and iron(II) centres occupy the axial positions; the crystal structure of the cationic cage is shown in Figure 6. On the other hand, reaction of **7** (1 equiv.) with $[Pd(CH_3CN)_4(BF_4)_2$ (0.75 equiv.) in acetonitrile yielded the corresponding tetradecanuclear $[Fe_8Pd_6]^{28+}$ cubic cage in which iron(II) centres are located at the corners of the cube while the six palladium(II) centres are positioned at the centre of each of the six sides.

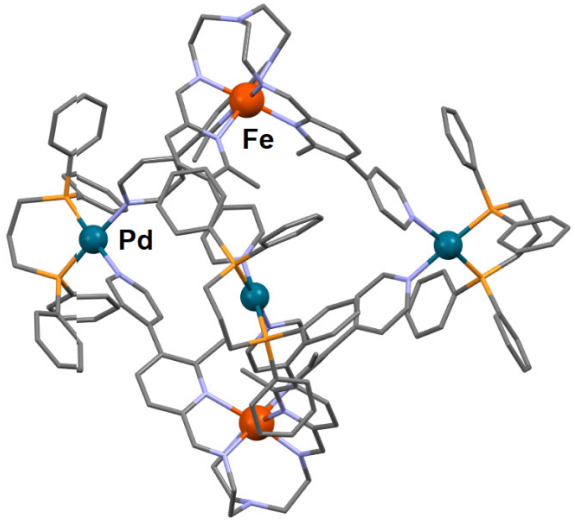

Figure 6. Crystal structure of the trigonal bipyramidal $[Fe_2Pd_3]^{10+}$ cage. Hydrogen atoms, tetraborate anions and solvent molecules are not shown [110].

Both these palladium(II)-containing products readily undergo dynamic subcomponent exchange reactions in solution. For example, the addition of sterically less-hindered ligand sub-components to particular hindered products transformed them to their corresponding low-spin analogues.

In a more recent report, Li and co-workers also described the assembly of a $[Fe_8Pd_6]^{28+}$, face-centred cubic cage [111]. Initially, the synthesis of the high-spin (S = 2) complex

$[FeL](BF_4)_2{\cdot}CH_3OH$ (where $[FeL]^{2+}$ = **8**) was undertaken, with an X-ray structure determination confirming its tripodal structure. In this case, the high-spin configuration arises directly from the weaker ligand field presented by the tris-imidazolimine derivative ligand employed.

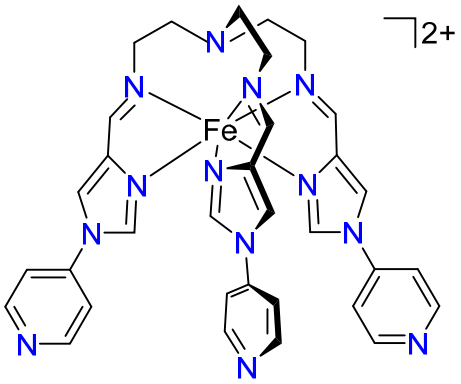

8

Reaction of $[FeL](BF_4)_2{\cdot}CH_3OH$ (4 equiv.) with $[Pd(CH_3CN)_4]^{2+}$ (3 equiv.) in acetonitrile resulted in formation of the cubic cage $[Fe_8Pd_6L_8](BF_4)_{28}$ in which the high-spin state of the respective iron(II) centres was preserved. Once again, this cationic cage has a face-centred cubic arrangement in which eight iron(II) centres, derived from eight metalloligands of type **8**, occupy the corners of the cube while a palladium(II) ion is positioned in the centre of each of the six faces [Figure 7a]. The crystal structure of the $[Fe_8Pd_6L_8]^{28+}$ cation (where $[FeL]^{2+}$ = **8**) is shown in Figure 7b. The iron(II) sites each retained a distorted octahedral coordination geometry with individual cages displaying either all Λ or all Δ chiral configurations at these sites; both enantiomeric isomers of the resulting cage occurred in the crystal lattice. The palladium(II) sites each adopted square planar coordination, being bound to four pyridyl nitrogen donors from four different **8** metalloligands. In this arrangement, all three pendent 4-pyridyl groups from each of eight metalloligands were utilised in cage formation. As might be expected, there was some degree of conformational rearrangement of the metalloligand **8** on forming the face-centred cubic product. For example, there was an eleven percent increase in the twist of each **8** on being incorporated into the cage structure.

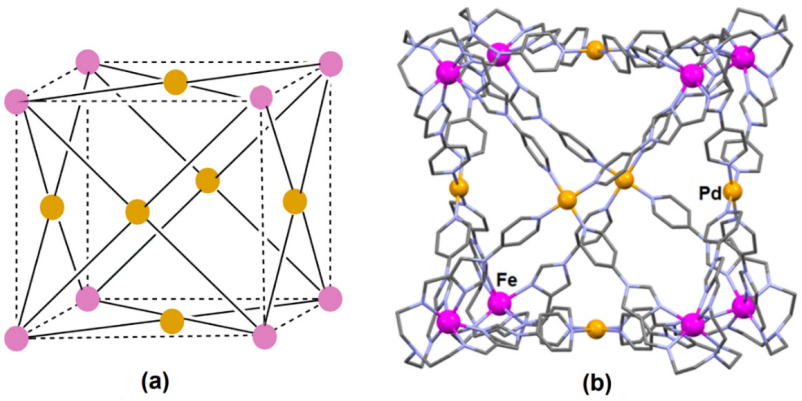

Figure 7. Structural details of the cubic cation in $[Fe_8Pd_6L_8](BF_4)_{28}$ (**9**) (where FeL = **8**). (**a**) Schematic representation of the metal ion sites in the face-centred cube. (**b**) Crystal structure of the cubic cation showing the octahedral coordination geometry of each iron(II) centre which is bound to six imidazole imine nitrogen donors and the square planar coordination of each palladium(II) site, which is bound to four pendent 4-pyridyl groups. Hydrogen atoms and BF_4^- anions are not shown [111].

Although a range of $[M_8M'_6]^{n+}$ cubic cages of the type just discussed have been reported, the majority of these were constructed employing centrosymmetric metalloligands. An example of cage formation employing a non-centrosymmetric metalloligand is given in a report by Zhang et al. [112]. These workers employed the Schiff-base condensation of tris(2-aminoethyl)amine with 4-imidazole carboxaldehyde in a 1:3 molar ratio followed by addition of yttrium(III) nitrate in slight excess to obtain the metalloligand $[Y(H_3L)(NO_3)](NO_3)_2$ (**10**) (where H_3L is the above tris-imine Schiff base condensation product). The absence of centrosymmetry in the $[Y(H_3L)(NO_3)]^{2+}$ cation is a direct consequence of the non-symmetric coordination shell of its yttium(III) centre which is bound to the above (heptadentate) Schiff base ligand as well as to a bidentate nitrato group. The overall coordination geometry of the yttium(III) centre is distorted capped square antiprismatic. The tripodal nature of the product (in its triply deprotonated form) indicating the tripodal arrangement of its coordination vectors is shown in Figure 8.

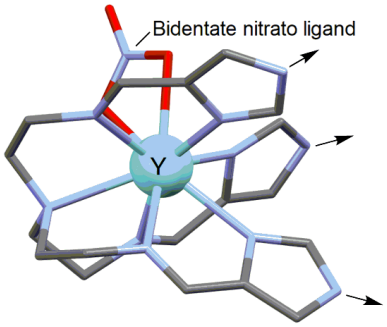

Figure 8. Schematic representation of the nine-coordinate, triply-deprotonated form of metalloligand **10** (the figure is derived from the crystal structure of its triply protonated form) [112]. The arrows indicate the distorted tripodal arrangement of the metalloligand's coordination vectors prior to binding to a (secondary) metal ion centre.

Reaction of **10** with copper(II) nitrate in methanol in the presence of triethylamine (as base) yielded a heterometallic (Cu^{II}/Y^{III}) cationic MOC of composition $[Cu_6Y_8L_8(NO_3)_5(H_2O)_3]^{7+}$. This product was the first reported heterometallic cage to contain yttrium(III). Of the eight yttrium(III) centres located at the corners of a distorted cube, five are nine-coordinate (and include the coordination of a bidentate nitrato ligand) while three are eight-coordinate (and include a coordinated water molecule). The crystal structure (see Figure 9) shows the manner in which the eight metalloligands of type **10** are linked to the six copper(II) sites; each of the three imidazolate groups from an individual metalloligand bind to three (adjacent) copper(II) sites. Five-coordinate copper(II) centres cap each of the six faces. Four of these centres are also bound to water molecules while two (on opposing sides of the cube) bind to monodentate nitrato groups (with the latter groups being severely disordered and not able to be fully modelled in the X-ray analysis).

Building on a prior study [113], Crowley and co-workers employed a stepwise procedure involving **11**, incorporating both monodentate (pyridyl) and bidentate (pyridyl and 1,2,3-triazole moiety) metal-binding sites, to generate the Pt(II) metalloligand (**12**) in which Pt(II) occupies the bidentate binding sites of two **11** ligands. The trans-planar configuration of **12** was confirmed by X-ray diffraction. In turn, **12** was used to construct the heterometallic Pd(II)/Pt(II) MOC (**13**) (see Figure 10) [113]. This study featured the innovative exploitation of the different kinetic liabilities of the Pd(II) and Pt(II) square planar d^8 ions, with the use of the relatively kinetically inert Pt(II) ion to "fix" this ion in metalloligand **12** while subsequently adding the more labile Pd(II) ion to complete the assembly of an open-sided heterometallic cage **13** in the absence of metal-ion "scrambling". This nona-nuclear (Pd_3Pt_6) heterometallic cage, in which both metal ion types contribute to its structural framework, has three large clefts. Cage **13** readily takes up anthracene guest molecules and, on being exposed to light, catalyses their conversion to endoperoxides (via

singlet oxygen generation). However, unfortunately this cage was found to be photolabile, leading to its eventual decomposition.

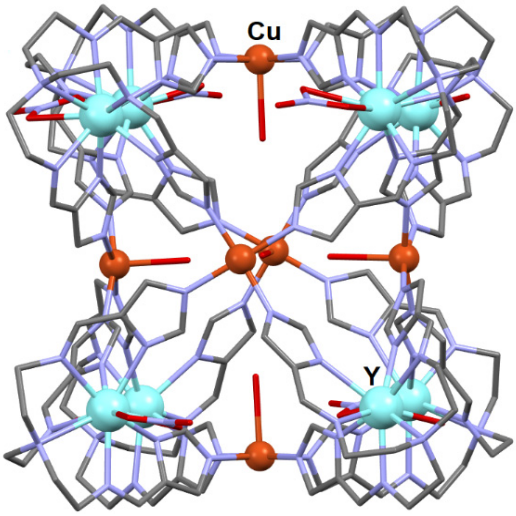

Figure 9. The crystal structure of the cationic cage $[Cu_6Y_8L_8(NO_3)_5(H_2O)_3]^{7+}$ [112].

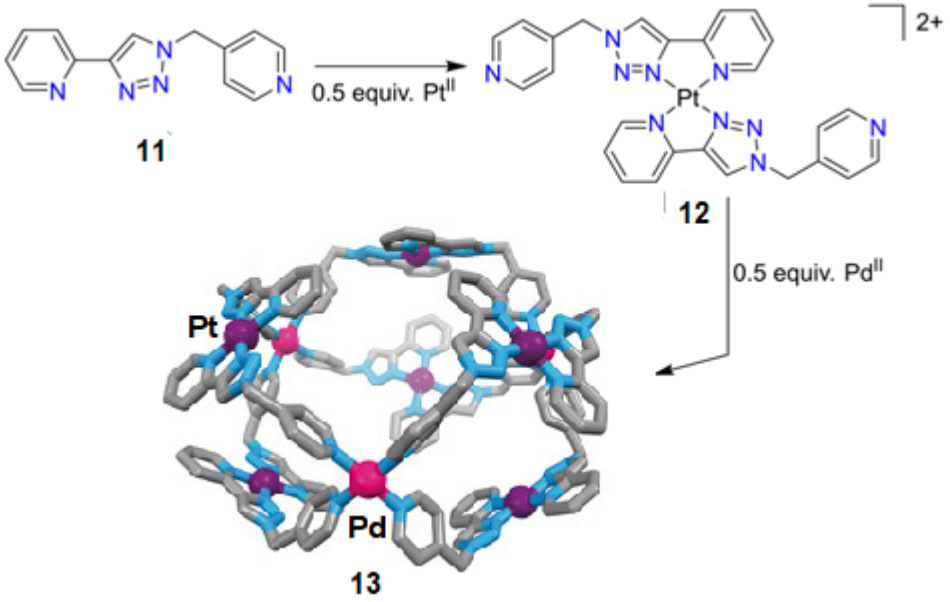

Figure 10. Metalloligand synthesis of the nona-nuclear heterometallic (Pd_3Pt_6) cage **13**. Structure **13** was reproduced (and adapted) from reference [114] with permission.

An attempt to form the corresponding all-palladium(II) cage by addition of $[Pd(CH_3CN)_4](BF_4)_2$ to **11** in acetonitrile in the required ratio initially failed to result in a "clean" synthesis, resulting instead in a complex equilibrium mixture being generated. The latter was attributed to the larger number of permutations available in the absence of the relatively inert platinum(II) sites. Nevertheless, allowing the above mixture to stand overnight did result in single crystals of a corresponding Pd^{II}_9 cage forming. This product was also observed to have a donut-like structure in which the palladium(II) ions now occupied two different coordination sites.

2.2. Cage Assembly Employing Clathrochelate Metalloligand Systems

In a long series of studies, Severin et al. have demonstrated that diamagnetic iron(II) clathrochelates, of which **14** and **15** represent trifunctional examples, are versatile metalloligands that have proved ideal for use in constructing large supramolecular assemblies that

include MOCs [115–118]. Such boron-capped iron(II) metalloligands have been demonstrated to be quite kinetically and thermodynamically stable species, properties that have aided their successful use in wide ranging studies by the above group. For example, the group has employed the trifunctional metalloligands **14** and **15** for the assembly of two large Pd_6L_6 cages, with these products being characterised by high molecular weights, as well as incorporating extended Pd–Pd distances [119].

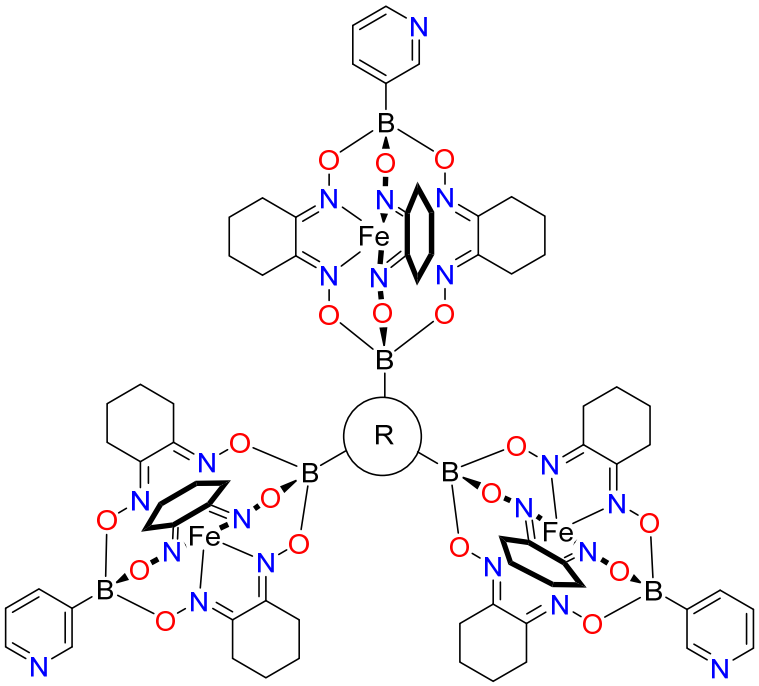

14: R = C_6H_3
15: R = $C_6H_3(C_6H_4)_3$

Each of **14** and **15** was readily synthesised via a one-pot synthesis. The triangular shape and the restricted flexibilities of these metalloligands are important design attributes contributing to both the predictability (and success!) of the subsequent assembly processes employed in this study. We note that the iron(II) centres are an integral part of these metalloligands and thus play an essential role in the orientation of the respective pyridyl coordination vectors.

It was noted by the above authors that the interaction of palladium(II) with other divergent tritopic ligand systems has commonly resulted in the formation of assemblies of type $Pd_{3n}L_{4n}$. The smallest member of the series, Pd_3L_4, is only able to form if some of the ligands act as chelating units [119,120] thus allowing the preferred square planar coordination geometry of each palladium(II) centre to be achieved. In the absence of chelate formation, cage assembly will involve a minimum of six palladium(II) ions and eight ligands. Guided by this, Severin et al. employed each of the trifunctional **14** and **15** metalloligands for cage formation, noting that the widely separated pyridyl nitrogen donors in each structure are not sterically aligned for chelate formation to occur. The triangular crystal structures of **14** and **15** were each confirmed by single-crystal X-ray diffraction studies [119].

Reaction of **14** or **15** with $[Pd(CH_3CN)_4](BF_4)_2$ in dimethyl sulfoxide (DMSO) led to formation of the corresponding **16** and **17** cages of type $[Pd_6L_8](BF_4)_{12}$ (L = **14** or **15**) with the crystal structure of **16** being confirmed by X-ray diffraction (Figure 11). Each of the six palladium(II) centres was located at the vertices of an octahedron, with each triangular

metalloligand spanning three adjacent palladium(II) centres such that they "panel" each of the eight faces.

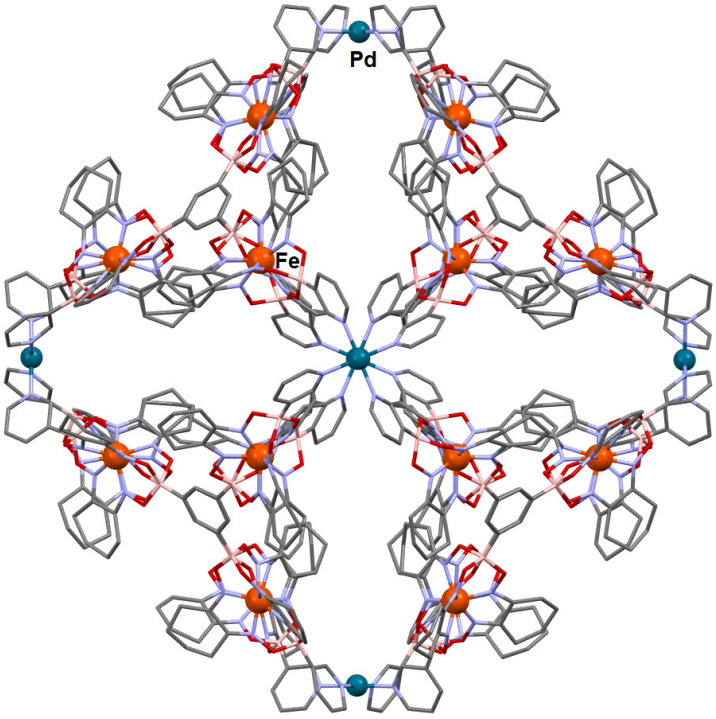

Figure 11. The crystal structure of $[Pd_6L_8](BF_4)_{12}$ (L = **14)** [119].

The size of the cavity in **16** was estimated to be 2·8 × 10^3 Å along with a Pd–Pd separation of 3·3 nm; these values corresponded to the largest cage of type M_6L_n (M = Pd, Pt) listed in the CCDC at the time of publication. This impressive result represents an exemplar of how the use of appropriately designed tripodal metalloligands can be used to extend the boundaries of existing cage chemistry in a rational manner.

In a different study the Severin group initially employed a virtual combinatorial library strategy that involved the mixing of equimolar amounts of six different dipyridyl ligands in which the 3- or 4-pyridyl groups are present in terminal positions and connected by rigid or semi-rigid linkers together with $[Pd(CH_3CN)_4](BF_4)_2$ (1 equiv.) in CD_3CN/CD_3NO_2 (4:1) [121]. Analysis of the resulting mixture indicated the preferential formation of a heteroleptic cage of type $[Pd_6L_6L'_6]^{12+}$. Motivated by this outcome the Severin group then probed whether a metalloligand approach might also be employed to generate a related (larger) cage of similar stoichiometry. With this as the goal, the group subsequently employed a combination of the previously reported clathrochelate metalloligands **18** and **19** (see Figure 12) as dipyridyl-containing analogues of the all-organic dipyridyl derivatives mentioned above [121].

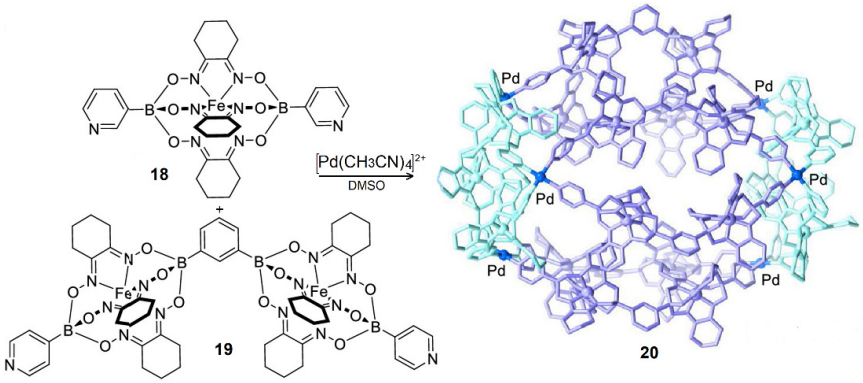

Figure 12. Structures of metalloligands **18** and **19** and the resulting $[Pd_6L_6L'_6]^{12+}$ cage **20**. Adapted with permission from [121]. Copyright (2021) American Chemical Society.

The group was successful in assembling the significantly larger $[Pd_6L_6L'_{6'}]^{12+}$ cage **20** employing the two clathrochelate metalloligands, **18** and **19**; **20** was isolated as its tetrafluoroborate salt. The synthetic procedure involved heating equimolar amounts of **18** and **19** with $[Pd(CH_3CN)_4](BF_4)_2$ in DMSO; NMR and ESI-MS results were consistent with formation of the target $[Pd_6L_6L'_6]^{12+}$ (L = **18**; L′ = **19**) cage. While single crystals of this product were isolated from DMSO, they yielded poor-quality X-ray diffraction data. Nevertheless, the data enabled the positions of the metal sites to be discerned as well as showing that the cationic cage adopted a prolate spheroid shape. The X-ray results coupled with MMFF computations confirmed that the structure of this cationic cage consisted of two $[Pd_3L_3]^{6+}$ (L = **18**) metallocycles linked by six **19** metalloligands to yield a trigonal prismatic arrangement (see Figure 12).

2.3. Cage Assembly Associated with In Situ Metalloligand Formation Involving a Metal-Ion Template Process

The use of mixed metals that undertake dual templating roles in the assembly of a heteronuclear metallocage was elegantly demonstrated in a study by Nitschke et al. [122]. This group demonstrated that reaction of three equivalents of 2-formal-8-aminoquinoline (**20**) with four equivalents of each of lanthanum(III) and zinc(II) in acetonitrile resulted in the assembly of the large heteronuclear cationic cage **21** (see Figure 13). In the assembly process it was predicted that the larger ionic radius of lanthanum(III) would promote a metal template reaction involving three molecules of **20** to yield the corresponding lanthanum(III), 18-membered macrocyclic species for use as the metalloligand (see Figure 14). Once formed, the latter incorporates a fully conjugated hexa-aza "inner" ring linked to three pendent triazole-pyridine units. Four molecules of this substituted macrocyclic species thus have available twelve pendent triazole-pyridine units for coordination to four (6-coordinate) zinc(II) ions. The fully conjugated macrocyclic core in this metal complex species undoubtedly displays both exceptional kinetic and thermodynamic stability due to the operation of the macrocyclic effect [123–125]. In the tetrahedral cage product, which was isolated as either its triflate or perchlorate salt, four lanthanum(III) macrocyclic structures occupy (as anticipated) the four sides of the resulting tetrahedral cage while the zinc(II) ions effectively "lock" the structure in place by occupying each of its four vertices.

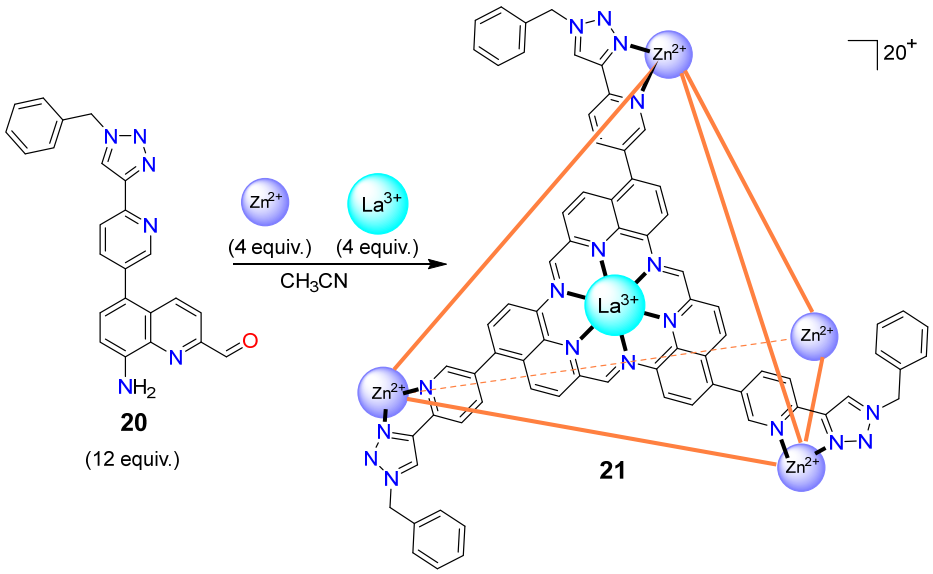

Figure 13. Two metal-ion-directed self-assembly of tetrahedron **21** from 2-formal-8-aminoquinoline (**20**) involving in situ metalloligand assembly. For clarity, only one face of **21** is shown [122].

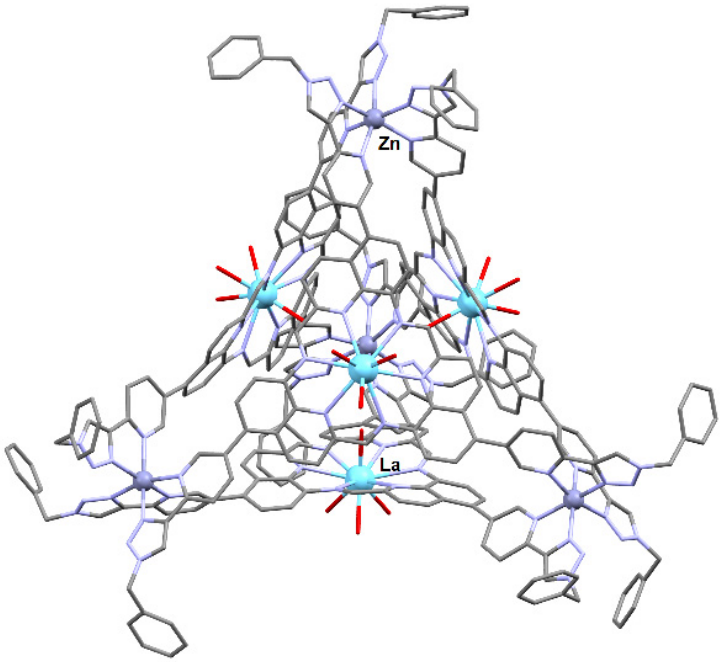

Figure 14. Crystal structure of the cationic cage **21**. Hydrogen atoms and perchlorate anions (which are present both inside and outside the cage cavity) are not shown [122].

Notably, when a single template ion [either lanthanum(III) or zinc(II)] was employed in a parallel synthesis, no cage was generated in either case. This is in accord with the complementary (and specific) template roles of the individual heterometal ions needed for successful cage formation. The crystal structure of this remarkable example of a metal-templated assembly of a specifically designed organic sub-component coupled with carefully selected metal ions is shown in Figure 14. In the product cage the macrocyclic faces were not flat but were somewhat "domed" such that each lanthanum(III) ion lay 0.64 Å out of the centre of its macrocyclic plane, while also being coordinated to four water molecules (shown as red sticks in Figure 14). The vertices, as well as the faces of **21** exhibited single handedness, resulting in *I* point symmetry. Clearly, this study suggests an innovative path-

way for obtaining further interesting heterometal cages incorporating other combinations of *d*-block and *f*-block ions.

3. Concluding Remarks

The use of the metalloligand approach for the directed assembly of MOCs remains a common strategy for generating metallocages. It represents an approach in which the steric and electronic information in both the chosen metal ion and the organic component(s) bear a complementary relationship that promotes the overall self-assembly process, leading to cage formation. Importantly, the use of a pre-organised metalloligand in such a process puts entropy on the side of the practitioner. In this context, kinetic inertness (with respect to metal exchange) coupled with moderate flexibility around the positions of the donor sites can often be desirable metalloligand design features. Clearly, there remains much scope for the continuing creative design and synthesis of new metalloligands that are able to influence both the form and the function of the MOCs that result.

Author Contributions: All authors contributed to the conception, writing, and editing of the manuscript. All authors have read and agreed to the published version of the manuscript.

Funding: This research received no external funding.

Institutional Review Board Statement: Not applicable.

Informed Consent Statement: Not applicable.

Data Availability Statement: Not applicable.

Acknowledgments: F.L. would like to thank Western Sydney University (WSU) for research support.

Conflicts of Interest: The authors declare no conflict of interest.

References

1. Saalfrank, R.W.; Stark, A.; Peters, K.; Vonschnering, H.G. Adamantoid chelate complexes. 1. The first adamantoid alkaline-earth metal chelate complex—Synthesis, structure, and reactivity. *Angew. Chem. Int. Ed.* **1988**, *27*, 851–853. [CrossRef]
2. Zhu, X.-W.; Luo, D.; Zhou, X.-P.; Li, D. Imidazole-based metal-organic cages: Synthesis, structures, and functions. *Coord. Chem. Rev.* **2022**, *455*, 214354. [CrossRef]
3. Virovets, A.V.; Peresypkina, E.; Scheer, M. Structural chemistry of giant metal based supramolecules. *Chem. Rev.* **2021**, *121*, 14485–14554. [CrossRef] [PubMed]
4. Gosselin, A.J.; Rowland, C.A.; Bloch, E.D. Permanently microporous metal—Organic polyhedra. *Chem. Rev.* **2020**, *120*, 8987–9014. [CrossRef]
5. Lindoy, L.F. Tetrahedral metallocages assembled from oligopyridine ligands and transition metal ions. *J. Incl. Phenom. Macrocycl. Chem.* **2019**, *94*, 121–131. [CrossRef]
6. Chakraborty, S.; Newkome, G.R. Terpyridine-based metallosupramolecular constructs: Tailored monomers to precise 2D-motifs and 3D-metallocages. *Chem. Soc. Rev.* **2018**, *47*, 3991–4016. [CrossRef]
7. Vasdev, R.A.S.; Preston, D.; Crowley, J.D. Multicavity metallosupramolecular architectures. *Chem. Asian J.* **2017**, *12*, 2513–2523. [CrossRef] [PubMed]
8. Amouri, H.; Desmarets, C.; Moussa, J. Confined nanospaces in metallocages: Guest molecules, weakly encapsulated anions, and catalyst sequestration. *Chem. Rev.* **2012**, *112*, 2015–2041. [CrossRef]
9. Davis, A.V.; Fiedler, D.; Seeber, G.; Zahl, A.; van Eldik, R.; Raymond, K.N. Guest exchange dynamics in an M_4L_6 tetrahedral host. *J. Am. Chem. Soc.* **2006**, *128*, 1324–1333. [CrossRef]
10. Kedia, M.; Shankar, B.; Sathiyendiran, M. Rhenium (I)-based neutral coordination cages with a spherical cavity for selective recognition of fluoride. *Inorg. Chem.* **2022**, *61*, 14506–14510. [CrossRef] [PubMed]
11. O'Connor, H.M.; Tipping, W.J.; Vallejo, J.; Nichol, G.S.; Faulds, K.; Graham, D.; Brechin, E.K.; Lusby, P.J. Utilizing Raman spectroscopy as a tool for solid- and solution-phase analysis of metalloorganic cage host-guest complexes. *Inorg. Chem.* **2022**, accepted. [CrossRef]
12. Zhu, C.; Yang, K.; Wang, H.; Fang, Y.; Feng, L.; Zhang, J.; Xiao, Z.; Wu, X.; Li, Y.; Fu, Y.; et al. Enantioseparation in hierarchically porous assemblies of homochiral cages. *ACS Central Sci.* **2022**, *8*, 562–570. [CrossRef] [PubMed]
13. Jackson, G.D.; Tipping, M.B.; Taylor, C.G.P.; Piper, J.R.; Pritchard, C.; Mozaceanu, C.; Ward, M.D. A family of externally-functionalised coordination cages. *Chemistry* **2021**, *3*, 88. [CrossRef]
14. Kieffer, M.; Bilbeisi, R.A.; Thoburn, J.D.; Clegg, J.K.; Nitschke, J.R. Guest binding drives host redistribution in libraries of $Co^{II}{}_4L_4$ cages. *Angew. Chem. Int. Ed.* **2020**, *59*, 11369–11373. [CrossRef]
15. Taylor, C.G.P.; Argent, S.P.; Ludden, M.D.; Piper, J.R.; Mozaceanu, C.; Barnett, S.A.; Ward, M.D. One Guest or Two? A crystallographic and solution study of guest binding in a cubic coordination cage. *Chem. Eur. J.* **2020**, *26*, 3054–3064. [CrossRef]

16. Kim, T.Y.; Vasdev, R.A.S.; Preston, D.; Crowley, J.D. Strategies for reversible guest uptake and release from metallosupramolecular architectures. *Chem. Eur. J.* **2018**, *24*, 14878–14890. [CrossRef] [PubMed]
17. Zhang, H.-N.; Lu, Y.; Gao, W.-X.; Lin, Y.-J.; Jin, G.-X. Selective Encapsulation and separation of dihalobenzene isomers with discrete heterometallic macrocages. *Chem. Eur. J.* **2018**, *24*, 18913–18921. [CrossRef]
18. Roukala, J.; Zhu, J.F.; Giri, C.; Rissanen, K.; Lantto, P.; Telkki, V.V. Encapsulation of xenon by a self-assembled Fe_4L_6 metallosupramolecular cage. *J. Am. Chem. Soc.* **2015**, *137*, 2464–2467. [CrossRef]
19. Schmidt, A.; Casini, A.; Kuehn, F.E. Self-assembled M_2L_4 coordination cages: Synthesis and potential applications. *Coord. Chem. Rev.* **2014**, *275*, 19–36. [CrossRef]
20. Jiao, Y.; Wang, J.; Wu, P.; Zhao, L.; He, C.; Zhang, J.; Duan, C. Cerium-based M_4L_4 tetrahedra as molecular flasks for selective reaction prompting and luminescent reaction tracing. *Chem. Eur. J.* **2014**, *20*, 2224–2231. [CrossRef]
21. Zhang, J.; Yu, H.; Zhang, C.; He, C.; Duan, C. Cerium-based M_4L_4 tetrahedrons containing hydrogen bond groups as functional molecular flasks for selective reaction prompting. *New J. Chem.* **2014**, *38*, 3137–3145. [CrossRef]
22. Clegg, J.K.; Li, F.; Jolliffe, K.A.; Meehan, G.V.; Lindoy, L.F. An expanded neutral M_4L_6 cage that encapsulates four tetrahydrofuran molecules. *Chem. Commun.* **2011**, *47*, 6042–6044. [CrossRef]
23. Brzechwa-Chodzyńska, A.; Drożdż, W.; Harrowfield, J.; Stefankiewicz, A.R. Fluorescent sensors: A bright future for cages. *Coord. Chem. Rev.* **2021**, *434*, 213820. [CrossRef]
24. Hu, X.; Han, M.; Shao, L.; Zhang, C.; Zhang, L.; Kelley, S.P.; Zhang, C.; Lin, J.; Dalgarno, S.J.; Atwood, D.A.; et al. Self-assembly of a semiconductive and photoactive heterobimetallic metal-organic capsule. *Angew. Chem. Int. Ed.* **2021**, *60*, 10516–10520. [CrossRef]
25. Wezenberg, S.J. Light-switchable metal-organic cages. *Chem. Lett.* **2020**, *49*, 609–615. [CrossRef]
26. Jing, X.; He, C.; Yang, Y.; Duan, C. A Metal–organic tetrahedron as a redox vehicle to encapsulate organic dyes for photocatalytic proton reduction. *J. Am. Chem. Soc.* **2015**, *137*, 3967–3974. [CrossRef]
27. Scott, A.J.; Vallejo, J.; Sarkar, A.; Smythe, L.; Regincós Martí, E.; Nichol, G.S.; Klooster, W.T.; Coles, S.J.; Murrie, M.; Rajaraman, G.; et al. Exploiting host-guest chemistry to manipulate magnetic interactions in metallosupramolecular M_4L_6 tetrahedral cages. *Chem. Sci.* **2021**, *12*, 5134–5142. [CrossRef] [PubMed]
28. Capel Berdiell, I.; Hochdörffer, T.; Desplanches, C.; Kulmaczewski, R.; Shahid, N.; Wolny, J.A.; Warriner, S.L.; Cespedes, O.; Schünemann, V.; Chastanet, G.; et al. Supramolecular iron metallocubanes exhibiting site-selective thermal and light-induced spin-crossover. *J. Am. Chem. Soc.* **2019**, *141*, 18759–18770. [CrossRef] [PubMed]
29. Campanella, A.J.; Ozvat, T.M.; Zadrozny, J.M. Ligand design of zero-field splitting in trigonal prismatic Ni (ii) cage complexes. *Dalton Trans.* **2022**, *51*, 3341–3348. [CrossRef]
30. Li, L.; Craze, A.R.; Mustonen, O.; Zenno, H.; Whittaker, J.J.; Hayami, S.; Lindoy, L.F.; Marjo, C.E.; Clegg, J.K.; Aldrich-Wright, J.R.; et al. A mixed-spin spin-crossover thiozolylimine $Fe_4L_6^{8+}$ cage. *Dalton Trans.* **2019**, *48*, 9935–9938. [CrossRef] [PubMed]
31. Yang, Y.; Wu, Y.; Jia, J.H.; Zheng, X.Y.; Zhang, Q.; Xiong, K.C.; Zhang, Z.M.; Wang, Q.M. Enantiopure magnetic heterometallic coordination cubic cages $(M_8Cu_6^{II})$-Cu^{II} (M = Ni, Co). *Cryst. Growth Des.* **2018**, *18*, 4555–4561. [CrossRef]
32. McConnell, A.J. Spin-state switching in Fe (II) helicates and cages. *Supramol. Chem.* **2018**, *30*, 858–868. [CrossRef]
33. Struch, N.; Bannwarth, C.; Ronson, T.K.; Lorenz, Y.; Mienert, B.; Wagner, N.; Engeser, M.; Bill, E.; Puttreddy, R.; Rissanen, K.; et al. An octanuclear metallosupramolecular cage designed to exhibit spin-crossover behavior. *Angew. Chem. Int. Ed.* **2017**, *56*, 4930–4935. [CrossRef] [PubMed]
34. Sánchez-González, E.; Tsang, M.Y.; Troyano, J.; Craig, G.A.; Furukawa, S. Assembling metal-organic cages as porous materials. *Chem. Soc. Rev.* **2022**, *51*, 4876–4889. [CrossRef]
35. Bell, D.J.; Natrajan, L.S.; Riddell, I.A. Design of lanthanide based metal-organic polyhedral cages for application in catalysis, sensing, separation and magnetism. *Coord. Chem. Rev.* **2022**, *472*, 214786. [CrossRef]
36. Pan, M.; Wu, K.; Zhang, J.H.; Su, C.Y. Chiral metal-organic cages/containers (MOCs): From structural and stereochemical design to applications. *Coord. Chem. Rev.* **2019**, *378*, 333–349. [CrossRef]
37. Ward, M.D.; Hunter, C.A.; Williams, N.H. Coordination cages based on bis (pyrazolylpyridine) ligands: Structures, dynamic behavior, guest binding, and catalysis. *Acc. Chem. Res.* **2018**, *51*, 2073–2082. [CrossRef]
38. Zhang, D.; Ronson, T.K.; Zou, Y.-Q.; Nitschke, J.R. Metal-organic cages for molecular separations. *Nat. Rev. Chem.* **2021**, *5*, 168–182. [CrossRef]
39. Zhu, J.; Yan, Z.; Bošković, F.; Haynes, C.J.E.; Kieffer, M.; Greenfield, J.L.; Wang, J.; Nitschke, J.R.; Keyser, U.F. $Fe^{II}_4L_4$ tetrahedron binds and aggregates DNA G-quadruplexes. *Chem. Sci.* **2021**, *12*, 14564–14569. [CrossRef]
40. Percástegui, E.G.; Ronson, T.K.; Nitschke, J.R. Design and applications of water-soluble coordination cages. *Chem. Rev.* **2020**, *120*, 13480–13544. [CrossRef]
41. Rizzuto, F.J.; von Krbek, L.K.S.; Nitschke, J.R. Strategies for binding multiple guests in metal-organic cages. *Nat. Rev. Chem.* **2019**, *3*, 204–222. [CrossRef]
42. Xu, N.; Tan, Y.X.; El-Sayed, E.S.M.; Yuan, D. Two zirconium metal-organic cages with S_4 and D_{2d} Symmetry: Construction and detection of antibiotics. *Cryst. Grow. Des.* **2022**, *22*, 2768–2773. [CrossRef]
43. Wei, L.; Ding, J.; Wu, J.; Li, L.; Li, Q.; Shao, L.-X.; Lu, J.; Qian, J. An efficient glucose sensor thermally calcined from copper-organic coordination cages. *Talanta* **2022**, *241*, 123263. [CrossRef] [PubMed]

44. Ma, Y.; Yang, X.; Leng, X.; Liu, X.; Schipper, D. A high-nuclearity Cd^{II}–Nd^{III} nanocage for the rapid ratiometric fluorescent detection of quercetin. *CrystEngComm* **2022**, *24*, 4534–4539. [CrossRef]
45. Ren, H.; Liu, C.; Yang, W.; Jiang, J. Sensitive and selective sensor based on porphyrin porous organic cage fluorescence towards copper ion. *Dye. Pigment.* **2022**, *200*, 110117. [CrossRef]
46. McTernan, C.T.; Davies, J.A.; Nitschke, J.R. Beyond platonic: How to build metal-organic polyhedra capable of binding low-symmetry, information-rich molecular cargoes. *Chem. Rev.* **2022**, *122*, 10393–10437. [CrossRef] [PubMed]
47. Li, W.Y.; Sun, L.; Liu, C.L.; Rotaru, A.; Robeyns, K.; Singleton, M.L.; Garcia, Y. Supramolecular $Fe^{II}{}_4L_4$ cage for fast ammonia sensing. *J. Mater. Chem. C* **2022**, *10*, 9216–9221. [CrossRef]
48. Yao, Y.; Li, J.Y.; Zhou, Y.Y.; Gao, T.; Li, H.F.; Yan, P.F. Turn-on luminescence detection of biogenic amine with an Eu (III) tetrahedron cage. *Dye. Pigment.* **2021**, *192*, 109441. [CrossRef]
49. Li, Y.-W.; Li, J.; Wan, X.-Y.; Sheng, D.-F.; Yan, H.; Zhang, S.-S.; Ma, H.-Y.; Wang, S.-N.; Li, D.-C.; Gao, Z.-Y.; et al. Nanocage-based N-rich metal-organic framework for luminescence sensing toward Fe^{3+} and Cu^{2+} ions. *Inorg. Chem.* **2021**, *60*, 671–681. [CrossRef]
50. Fang, Y.; Dehaen, W. Small-molecule-based fluorescent probes for *f*-block metal ions: A new frontier in chemosensors. *Coord. Chem. Rev.* **2021**, *427*, 213524. [CrossRef]
51. Zhang, Z.; Zhao, Z.; Wu, L.; Lu, S.; Ling, S.; Li, G.; Xu, L.; Ma, L.; Hou, Y.; Wang, X.; et al. Emissive platinum (II) cages with reverse fluorescence resonance energy transfer for multiple sensing. *J. Am. Chem. Soc.* **2020**, *142*, 2592–2600. [CrossRef] [PubMed]
52. Pilgrim, B.S.; Champness, N.R. Metal-organic frameworks and metal-organic cages—A perspective. *ChemPlusChem* **2020**, *85*, 1842–1856. [CrossRef]
53. Yao, Y.; Zhou, Y.Y.; Zhu, T.Y.; Gao, T.; Li, H.F.; Yan, P.F. Eu (III) tetrahedron cage as a luminescent chemosensor for rapidly reversible and turn-on detection of volatile amine/NH_3. *Acs Appl. Mat. Interfaces* **2020**, *12*, 15338–15347. [CrossRef] [PubMed]
54. Zhou, Z.X.; Liu, J.P.; Huang, J.J.; Rees, T.W.; Wang, Y.L.; Wang, H.; Li, X.P.; Chao, H.; Stang, P.J. A self-assembled Ru-Pt metallacage as a lysosome-targeting photosensitizer for 2-photon photodynamic therapy. *Proc. Natl. Acad. Sci. USA* **2019**, *116*, 20296–20302. [CrossRef]
55. Wang, Z.; Zhou, L.-P.; Zhao, T.-H.; Cai, L.-X.; Guo, X.-Q.; Duan, P.-F.; Sun, Q.-F. Hierarchical self-assembly and chiroptical studies of luminescent 4d–4f cages. *Inorg. Chem.* **2018**, *57*, 7982–7992. [CrossRef] [PubMed]
56. Wang, K.; Jordan, J.H.; Hu, X.-Y.; Wang, L. Supramolecular strategies for controlling reactivity within confined nanospaces. *Angew. Chem. Int. Ed.* **2020**, *59*, 13712–13721. [CrossRef]
57. Galan, A.; Ballester, P. Stabilization of reactive species by supramolecular encapsulation. *Chem. Soc. Rev.* **2016**, *45*, 1720–1737. [CrossRef]
58. Vardhan, H.; Verpoort, F. Metal-organic polyhedra: Catalysis and reactive intermediates. *Adv. Synth. Catal.* **2015**, *357*, 1351–1368. [CrossRef]
59. Mal, P.; Breiner, B.; Rissanen, K.; Nitschke, J.R. White phosphorus is air-stable within a self-assembled tetrahedral capsule. *Science* **2009**, *324*, 1697–1699. [CrossRef]
60. Fang, Y.; Powell, J.A.; Li, E.; Wang, Q.; Perry, Z.; Kirchon, A.; Yang, X.; Xiao, Z.; Zhu, C.; Zhang, L.; et al. Catalytic reactions within the cavity of coordination cages. *Chem. Soc. Rev.* **2019**, *48*, 4707–4730. [CrossRef]
61. Saha, R.; Mondal, B.; Mukherjee, P.S. Molecular cavity for catalysis and formation of metal nanoparticles for use in catalysis. *Chem. Rev.* **2022**, *122*, 12244–12307. [CrossRef]
62. Chen, S.; Chen, L.-J. Metal-organic cages: Applications in organic reactions. *Chemistry* **2022**, *4*, 36. [CrossRef]
63. Yu-Lin, L. A redox-active supramolecular Fe_4L_6 cage based on organic vertices with acid-base-dependent charge tunability for dehydrogenation catalysis. *J. Am. Chem. Soc.* **2022**, *144*, 8778–8788.
64. Taylor, C.G.P.; Ward, M.D. Supramolecular catalysis with a cubic coordination cage: Contributions from cavity and external-surface binding. *Supramol. Catal.* **2022**, 241–254. [CrossRef]
65. Zhou, S.; Zhang, Z.; Bai, D.; Li, J.; Cui, X.; Xu, Z.J.; Tang, Y.; Tang, X.; Liu, W. A Discrete 3d–4f metallacage as an efficient catalytic nanoreactor for a three-component aza-Darzens reaction. *Inorg. Chem.* **2022**, *61*, 4009–4017. [CrossRef] [PubMed]
66. Xue, Y.; Hang, X.; Ding, J.; Li, B.; Zhu, R.; Pang, H.; Xu, Q. Catalysis within coordination cages. *Coord. Chem. Rev.* **2021**, *430*, 213656. [CrossRef]
67. Yadav, S.; Kannan, P.; Qiu, G. Cavity-based applications of metallo-supramolecular coordination cages (MSCCs). *Org. Chem. Front.* **2020**, *7*, 2842–2872. [CrossRef]
68. Tan, C.; Chu, D.; Tang, X.; Liu, Y.; Xuan, W.; Cui, Y. Supramolecular coordination cages for asymmetric catalysis. *Chem. Euro. J.* **2019**, *25*, 662–672. [CrossRef] [PubMed]
69. Severinsen, R.J.; Rowlands, G.J.; Plieger, P.G. Coordination cages in catalysis. *J. Incl. Phenom. Macrocycl. Chem.* **2019**, *96*, 29–42. [CrossRef]
70. Gao, W.-X.; Zhang, H.-N.; Jin, G.-X. Supramolecular catalysis based on discrete heterometallic coordination-driven metallacycles and metallacages. *Coord. Chem. Rev.* **2019**, *386*, 69–84. [CrossRef]
71. Ward, M.D.; Raithby, P.R. Functional behaviour from controlled self-assembly: Challenges and prospects. *Chem. Soc. Rev.* **2013**, *42*, 1619–1636. [CrossRef] [PubMed]
72. Sinha, I.; Mukherjee, P.S. Chemical transformations in confined space of coordination architectures. *Inorg. Chem.* **2018**, *57*, 4205–4221. [CrossRef] [PubMed]

73. Brown, C.J.; Toste, F.D.; Bergman, R.G.; Raymond, K.N. Supramolecular catalysis in metal-ligand cluster hosts. *Chem. Rev.* **2015**, *115*, 3012–3035. [CrossRef] [PubMed]
74. Hastings, C.J.; Pluth, M.D.; Bergman, R.G.; Raymond, K.N. Enzyme-like catalysis of the Nazarov cyclization by supramolecular encapsulation. *J. Am. Chem. Soc.* **2010**, *132*, 6938–6940. [CrossRef]
75. Brown, C.J.; Bergman, R.G.; Raymond, K.N. Enantioselective catalysis of the aza-Cope rearrangement by a chiral supramolecular assembly. *J. Am. Chem. Soc.* **2009**, *131*, 17530–17531. [CrossRef]
76. Samanta, S.K.; Isaacs, L. Biomedical applications of metal organic polygons and polyhedra (MOPs). *Coord. Chem. Rev.* **2020**, *410*, 213181. [CrossRef]
77. Ahmad, N.; Younus, H.A.; Chughtai, A.H.; Verpoort, F. Metal-organic molecular cages: Applications of biochemical implications. *Chem. Soc. Rev.* **2015**, *44*, 9–25. [CrossRef]
78. Sokolow, G.E.; Crawley, M.R.; Morphet, D.R.; Asik, D.; Spernyak, J.A.; McGray, A.J.R.; Cook, T.R.; Morrow, J.R. Metal-organic polyhedron with four Fe (III) centers producing enhanced T1 magnetic resonance imaging contrast in tumors. *Inorg. Chem.* **2022**, *61*, 2603–2611. [CrossRef]
79. Liu, Y.-Y.; Yu, H.-J.; Wang, Y.-P.; Li, C.-J.; Wang, X.-F.; Ye, C.-G.; Yao, H.-L.; Pan, M.; Su, C.-Y. A photoactive Ir-Pd bimetallic cage with high singlet oxygen yield for efficient one/two-photon activated photodynamic therapy. *Mater. Chem. Front.* **2022**, *6*, 948–955. [CrossRef]
80. Lisboa, L.S.; Preston, D.; McAdam, C.J.; Wright, L.J.; Hartinger, C.G.; Crowley, J.D. Heterotrimetallic double cavity cages: Syntheses and selective guest binding. *Angew. Chem. Int. Ed.* **2022**, *61*, e202201700. [CrossRef]
81. Xu, W.Q.; Fan, Y.Z.; Wang, H.P.; Teng, J.; Li, Y.H.; Chen, C.X.; Fenske, D.; Jiang, J.J.; Su, C.Y. Investigation of binding behavior between drug molecule 5-fluoracil and M_4L_4-type tetrahedral cages: Selectivity, capture, and release. *Chem. Eur. J.* **2017**, *23*, 3542–3547. [CrossRef] [PubMed]
82. Preston, D.; Lewis, J.E.M.; Crowley, J.D. Multicavity PdnL4 (2n+) cages with controlled segregated binding of different guests. *J. Am. Chem. Soc.* **2017**, *139*, 2379–2386. [CrossRef] [PubMed]
83. Zheng, Y.R.; Suntharalingam, K.; Johnstone, T.C.; Lippard, S.J. Encapsulation of Pt (IV) prodrugs within a Pt (II) cage for drug delivery. *Chem. Sci.* **2015**, *6*, 1189. [CrossRef] [PubMed]
84. Lewis, J.E.M.; Gavey, E.L.; Cameron, S.A.; Crowley, J.D. Stimuli-responsive Pd_2L_4 metallosupramolecular cages: Towards targeted cisplatin drug delivery. *Chem. Sci.* **2012**, *3*, 778–784. [CrossRef]
85. McConnell, A.J. Metallosupramolecular cages: From design principles and characterisation techniques to applications. *Chem. Soc. Rev.* **2022**, *51*, 2957–2971. [CrossRef]
86. Hardy, M.; Lutzen, A. Better together: Functional heterobimetallic macrocyclic and cage-like assemblies. *Chem. Eur. J.* **2020**, *26*, 13332–13346. [CrossRef] [PubMed]
87. Pullen, S.; Tessarolo, J.; Clever, G.H. Increasing structural and functional complexity in self-assembled coordination cages. *Chem. Sci.* **2021**, *12*, 7269–7293. [CrossRef]
88. Sun, Y.; Chen, C.; Liu, J.; Stang, P.J. Recent developments in the construction and applications of platinum-based metallacycles and metallacages via coordination. *Chem. Soc. Rev.* **2020**, *49*, 3889–3919. [CrossRef] [PubMed]
89. Lewis, J.E.M.; Crowley, J.D. Metallo-supramolecular self-assembly with reduced-symmetry ligands. *ChemPlusChem* **2020**, *85*, 815–827. [CrossRef]
90. Li, H.; Yao, Z.J.; Liu, D.; Jin, G.X. Multi-component coordination-driven self-assembly toward heterometallic macrocycles and cages. *Coord. Chem. Rev.* **2015**, *293*, 139–157. [CrossRef]
91. Cook, T.R.; Stang, P.J. Recent developments in the preparation and chemistry of metallacycles and metallacages via coordination. *Chem. Rev.* **2015**, *115*, 7001–7045. [CrossRef] [PubMed]
92. Caulder, D.L.; Raymond, K.N. The rational design of high symmetry coordination clusters. *J. Chem. Soc. Dalton Trans.* **1999**, *8*, 1185–1200. [CrossRef]
93. Fujita, M.; Umemoto, K.; Yoshizawa, M.; Fujita, N.; Kusukawa, T.; Biradha, K. Molecular paneling via coordination. *Chem. Commun.* **2001**, *6*, 509–518. [CrossRef]
94. Zhou, M.-Y.; Tong, J.; Lu, H.-L.; Wang, X.-Y.; Yu, S.-Y. Hierarchical self-assembly and packing models of dipalladium (II,II)-based metallacapsules and metallacages based on amide-functionalized multi-pyrazoles. *Inorg. Chem. Commun.* **2022**, *136*, 109145. [CrossRef]
95. Fujita, M.; Ogura, K. Transition-metal-directed assembly of well-defined organic architectures possessing large voids: From macrocycles to 2-catenanes. *Coord. Chem. Rev.* **1996**, *148*, 249–264. [CrossRef]
96. Zhang, D.; Ronson, T.K.; Nitschke, J.R. Functional capsules via subcomponent self-assembly. *Acc. Chem. Res.* **2018**, *51*, 2423–2436. [CrossRef]
97. Li, F.; Lindoy, L.F. Metalloligand strategies for assembling heteronuclear nanocages—Recent developments. *Aust. J. Chem.* **2019**, *72*, 731–741. [CrossRef]
98. Rota Martir, D.; Zysman-Colman, E. Photoactive supramolecular cages incorporating Ru (II) and Ir (III) metal complexes. *Chem. Commun.* **2019**, *55*, 139–158. [CrossRef]
99. Zhang, Y.-Y.; Gao, W.-X.; Lin, L.; Jin, G.-X. Recent advances in the construction and applications of heterometallic macrocycles and cages. *Coord. Chem. Rev.* **2017**, *344*, 323–344. [CrossRef]
100. Pachisia, S.; Gupta, R. Tailored inorganic-organic architectures via metalloligands. *Chem. Rec.* **2022**, e202200121. [CrossRef]

101. Zhou, X.-C.; Wu, L.-X.; Wang, X.-Z.; Lai, Y.-L.; Ge, Y.-Y.; Su, J.; Zhou, X.-P.; Li, D. Self-assembly of a $Pd_4Cu_8L_8$ cage for epoxidation of styrene and its derivatives. *Inorg. Chem.* **2022**, *61*, 5196–5200. [CrossRef] [PubMed]
102. Martir, D.R.; Cordes, D.B.; Slawin, A.M.Z.; Escudero, D.; Jacquemin, D.; Warriner, S.L.; Zysman-Colman, E. A luminescent Pd4Ru8 (24+) supramolecular cage. *Chem. Commun.* **2018**, *54*, 6016–6019. [CrossRef] [PubMed]
103. Li, C.; Liu, Y.; Wang, Y.; Guo, J.; Pan, M. Assembly and properties of Pd_4Ru_8 metal-organic cages based on polypyridine Ru (II)-metalloligand. *Sci. Sin. Chim.* **2020**, *50*, 687–694.
104. Li, X.; Gorle, A.K.; Sundaraneedi, M.K.; Keene, F.R.; Collins, J.G. Kinetically-inert polypyridylruthenium(II) complexes as therapeutic agents. *Coord. Chem. Rev.* **2018**, *375*, 134–147. [CrossRef]
105. O'Connor, H.M.; Sanz, S.; Scott, A.J.; Pitak, M.B.; Klooster, W.T.; Coles, S.J.; Chilton, N.F.; McInnes, E.J.L.; Lusby, P.J.; Weihe, H.; et al. $(Cr^{III}{}_8Ni^{II}{}_6)^{n+}$ Heterometallic coordination cubes. *Molecules* **2021**, *26*, 757. [CrossRef]
106. Sanz, S.; O'Connor, H.M.; Comar, P.; Baldansuren, A.; Pitak, M.B.; Coles, S.J.; Weihe, H.; Chilton, N.F.; McInnes, E.J.L.; Lusby, P.J.; et al. Modular $[Fe^{III}8M^{II}{}_6]_n{}^+$ (M^{II} = Pd, Co, Ni, Cu) coordination cages. *Inorg. Chem.* **2018**, *57*, 3500–3506. [CrossRef]
107. O'Connor, H.M.; Sanz, S.; Pitak, M.B.; Coles, S.J.; Nichol, G.S.; Piligkos, S.; Lusby, P.J.; Brechin, E.K. $[Cr^{III}{}_8M^{II}{}_6]^{n+}$ (M^{II} = Cu, Co) face-centred, metallosupramolecular cubes. *CrystEngComm* **2016**, *18*, 4914–4920. [CrossRef]
108. Sanz, S.; O'Connor, H.M.; Pineda, E.M.; Pedersen, K.S.; Nichol, G.S.; Mønsted, O.; Weihe, H.; Piligkos, S.; McInnes, E.J.L.; Lusby, P.J.; et al. $[Cr^{III}{}_8M^{II}{}_6]^{12+}$ coordination cubes (MII = Cu, Co). *Angew. Chem. Int. Ed.* **2015**, *54*, 6761–6764. [CrossRef]
109. Hardy, M.; Struch, N.; Topić, F.; Schnakenburg, G.; Rissanen, K.; Lützen, A. Stepwise construction of heterobimetallic cages by an extended molecular library approach. *Inorg. Chem.* **2018**, *57*, 3507–3515. [CrossRef]
110. Hardy, M.; Struch, N.; Holstein, J.J.; Schnakenburg, G.; Wagner, N.; Engeser, M.; Beck, J.; Clever, G.H.; Lützen, A. Dynamic complex-to-complex transformations of heterobimetallic systems influence the cage structure or spin state of iron (II) ions. *Angew. Chem. Int. Ed.* **2020**, *59*, 3195–3200. [CrossRef]
111. Min, H.; Craze, A.R.; Taira, T.; Wallis, M.J.; Bhadbhade, M.M.; Tian, R.; Fanna, D.J.; Wuhrer, R.; Hayami, S.; Clegg, J.K.; et al. Self-assembly of a rare high spin Fe^{II}/Pd^{II} tetradecanuclear cubic cage constructed via the metalloligand approach. *Chemistry* **2022**, *4*, 38. [CrossRef]
112. Zhang, Y.J.; Harman, D.G.; Avdeev, M.; Karatchevtseva, I. Cu (II) ion directed self-assembly of a Y8/Cu6 heterometallic coordination cage via an Y (III) metalloligand. *Inorg. Chim. Acta* **2019**, *484*, 521–526. [CrossRef]
113. Preston, D.; Tucker, R.A.J.; Garden, A.L.; Crowley, J.D. Heterometallic $[M_nPt_n(L)_{2n}]^{x+}$ macrocycles from dichloromethane-derived bis-2-pyridyl-1,2,3-triazole ligands. *Inorg. Chem.* **2016**, *55*, 8928–8934. [CrossRef] [PubMed]
114. Preston, D.; Sutton, J.J.; Gordon, K.C.; Crowley, J.D. A nona-nuclear heterometallic Pd_3Pt_6 "donut"-shaped cage: Molecular recognition and photocatalysis. *Angew. Chem. Int. Ed.* **2018**, *57*, 8659–8663. [CrossRef] [PubMed]
115. Planes, O.M.; Schouwink, P.A.; Bila, J.L.; Fadaei-Tirani, F.; Scopelliti, R.; Severin, K. Incorporation of clathrochelate-based metalloligands in metal-organic frameworks by solvent-assisted ligand exchange. *Cryst. Growth Des.* **2020**, *20*, 1394–1399. [CrossRef]
116. Giraldi, E.; Depallens, A.B.; Ortiz, D.; Fadaei-Tirani, F.; Scopelliti, R.; Severin, K. Boronate ester-capped helicates. *Chem. Eur. J.* **2020**, *26*, 7578–7582. [CrossRef]
117. Bila, J.L.; Pijeat, J.; Ramorini, A.; Fadaei-Tirani, F.; Scopelliti, R.; Baudat, E.; Severin, K. Porous networks based on iron (II) clathrochelate complexes. *Dalton Trans.* **2019**, *48*, 4582–4588. [CrossRef]
118. Jansze, S.M.; Severin, K. Clathrochelate metalloligands in supramolecular chemistry and materials science. *Acc. Chem. Res.* **2018**, *51*, 2139–2147. [CrossRef]
119. Jansze, S.M.; Ortiz, D.; Fadaei Tirani, F.; Scopelliti, R.; Menin, L.; Severin, K. Inflating face-capped Pd_6L_8 coordination cages. *Chem. Commun.* **2018**, *54*, 9529–9532. [CrossRef]
120. Ronson, T.K.; Carruthers, C.; Fisher, J.; Brotin, T.; Harding, L.P.; Rizkallah, P.J.; Hardie, M.J. Tripodal 4-pyridyl-derived host ligands and their metallo-supramolecular chemistry: Stella octangula and bowl-shaped assemblies. *Inorg. Chem.* **2010**, *49*, 675–685. [CrossRef]
121. Sudan, S.; Li, R.-J.; Jansze, S.M.; Platzek, A.; Rudolf, R.; Clever, G.H.; Fadaei-Tirani, F.; Scopelliti, R.; Severin, K. Identification of a heteroleptic $Pd_6L_6L'_6$ coordination cage by screening of a virtual combinatorial library. *J. Am. Chem. Soc.* **2021**, *143*, 1773–1778. [CrossRef] [PubMed]
122. Yang, D.; Greenfield, J.L.; Ronson, T.K.; von Krbek, L.K.S.; Yu, L.; Nitschke, J.R. La-III and Zn-II cooperatively template a metal-organic capsule. *J. Am. Chem. Soc.* **2020**, *142*, 19856–19861. [CrossRef] [PubMed]
123. Cabbiness, D.K.; Margerum, D.W. Macrocyclic effect on the stability of copper (II) tetramine complexes. *J. Am. Chem. Soc.* **1969**, *91*, 6540–6542. [CrossRef]
124. Cabbiness, D.K.; Margerum, D.W. Effect of macrocyclic structures on the rate of formation and dissociation of copper (II) complexes. *J. Am. Chem. Soc.* **1970**, *92*, 2151–2153. [CrossRef]
125. Lindoy, L.F. *The Chemistry of Macrocyclic Ligand Complexes*; Cambridge University Press: Cambridge, UK, 1989.